Aerodynamic drag reduction by means of platooning configurations of light commercial vehicles: A flow field analysis

Aerodynamic drag reduction by means of platooning configurations of light commercial vehicles: a flow field analysis

J.J. Cerutti[1], G. Cafiero[1,2,*], G. Iuso[1]

[1]Department of Mechanical and Aerospace Engineering, Flow Control Group, Politecnico di Torino, Corso Duca degli Abruzzi 24, 10129, Torino (Italy)

[2]Centre for Aerodynamics and Environmental Flow, Department of Mechanical Engineering Sciences, University of Surrey, GU2 7HX, Guildford (UK)

[*] Corresponding Author: gioacchino.cafiero@polito.it

Keywords: platooning, drag reduction, 3D wake dynamics.

Abstract

Platooning configurations of two, three and four commercial vehicles were tested at a Reynolds number based on the vehicle's length (L) of 230000. The platoon configurations were obtained using an instrumented model, and three wooden replicas located at different positions with respect to the instrumented one. The reference model presents a slant angle at the leading edge, which can produce, in principle, a significantly different flow field compared to the generally studied Ahmed body. Drag, static pressure distributions and pressure fluctuations measurements were carried out. Additionally, planar PIV measurements were performed to investigate the near wake of the two-vehicles platoon configuration.
For the two-models platoon, drag reductions of 30% and 43% were evidenced for the front and for the rear vehicle, respectively, at an inter-vehicle distance (d) equal to half the vehicle's length, and corresponding to an average drag reduction of 36.5%. For increasing distance, the benefit associated with the platooning configuration reduces, reaching an average drag reduction of 20% at d/L=3. We relate the vehicle's drag to the flow field organization and to the distribution of the modal energy through Proper Orthogonal Decomposition of the microphonic probes located on the base of the instrumented vehicle. We also evidence that the key element that is responsible for the pumping of the wake is the large vortex that generates near the top edge of the vehicle's base.
We show that the slant angle does not affect the drag reduction of the leading vehicle of the platoon, whereas it can lead to larger differences in the case of the rear vehicle.

For three and four-vehicles platoons, consistently larger values of the average drag reduction are experienced ($\approx$ 35%) and were also obtained for distances larger than $1L$. A simple model describing the overall drag reduction for a generic number of vehicles is presented and discussed.

1. Introduction

The ambitious goals set by the European Union to achieve significant reductions of the pollution and sound emission throughout the entire transportation market have stimulated flourishing research in the field. The interest is strongly cross-disciplinary and requires efforts at different levels. Examples can be found in the air transportation, where engine and airframe manufacturers are pushing towards distributed propulsion, with significant benefit in terms of emissions and sound pollution.

However, a large share of the commercial routes in Europe still heavily relies on the road transportation. It is estimated that the 45.9% of the goods are moved across Europe using light and heavy commercial vehicles accounting for the 30% of the total transport energy use (Bonilla 2020). It is then mandatory to identify innovative approaches to tackle the pollution associated with a such large volume of vehicles.

In this field, the increasing capabilities of artificial intelligence has provided a strong push towards the development of autonomous driving. The application of these new developments paves the way towards the implementation of the "platoon" marching of heavy vehicles. Platoon marching is generally referred to as the case of a convoy of a given number of vehicles that are marching in a line.

While this feature is extensively employed in motorsport, where it is generally referred to as slipstreaming, as well as by cyclists, the hazard associated with the close proximity of the vehicles hinders its implementation for commercial vehicles.

A pioneering study of the aerodynamics of the platooning configuration was performed by Zabat et al. (1995). Drag reductions of both the leading and trailing model were evidenced for inter-vehicle distances (d) smaller than the vehicle's length (L). The authors also evidenced that the drag reduction of the leading model disappears when $d/L > 1$.

Even though numerous investigations have shown its potential benefits (Michaelian & Browand (2000), Tsuei & Savas, (2010) , Davila et al. (2013), Vegendla et al. (2015), Salari & Ortega (2018), Hamiga & Ciesielka (2018), to cite some), the main concern arises from the fact that the largest drag reductions are evidenced at short inter-vehicle spacings, with potential risks associated with the response time in case of emergency. As mentioned, developments in autonomous driving and control (Gehring & Fritz (2002), Alam et al. (2013), Al Alam et al. (2011), Bergenhem et al. (2012), Yu et al. (2016) to cite some) will enable the large-scale implementation of this methodology, with the associated renewed interest in the understanding of the underlying physics leading to drag reduction, particularly from the aerodynamics point of view.

Under some specific platoon configurations, the resulting aerodynamic performance may actually worsen, as demonstrated by the investigations by Pagliarella et al. (2007) and Watkins & Vino (2008). The authors investigated a range of geometry modifications on the typical Ahmed body. In particular, they looked at the effect of the slant angle and they investigated a range of configurations where the leading and rear model had pre-critical (smaller than 30^o) and post-critical (larger than 30^o) values of the slant angle. The authors also argued that the drag reductions experienced on the rear vehicle are progressively reduced as a consequence of the pressure increase associated with the large vortices shed by the leading vehicle, impinging on the front surface.

More recently, a joint experimental and large eddy simulations (LES) study by Uystepruyst & Krajnović (2013) evidenced potential benefit for the vehicles in a platoon of four cuboids at small values of the inter-vehicle distance. Other numerical efforts, requiring less computational power and based on the use of detached eddy simulations (DES), allowed the investigation of a much larger platoon (8 vehicles) with an inter-vehicle spacing of $0.5L$. They showed good agreement with the available experimental results obtained with moving models rather than in wind tunnel tests (He et al. 2019). The authors evidenced large values of the drag reduction for all the intermediate vehicles, with an associated highly turbulent flow.

Despite the large number of investigations that have dealt with the problem, many of them have typically focused on the effect of the platooning configuration on the drag coefficient, with lower interest on the statistical description of the resulting flow field for a broad range of inter-vehicle distances.

In this paper, we aim at addressing the following aspects: for a 1:10 scale model of a commercial light vehicle, with a leading edge slant angle, what is the effect of the platooning configuration on the drag coefficient of the single models, as well as the overall drag coefficient of the platoon? What is the effect of the platoon configuration on the wake dynamics and its structure, as a function of the inter-vehicle distance? Both from the flow field data obtained with particle image velocimetry and from the proper orthogonal decomposition of the microphonic probes we are interested in determining the leading mechanism driving the drag variation as a function of the inter-vehicle distance. Furthermore, comparing our results with the literature, we can draw some conclusions on the effect of the slant angle on the drag reduction of the platoon.

Besides providing relevant information on the overall drag reduction, the flow field organization of the near wake of vehicles marching in platoon configuration at different inter-vehicle distances is of paramount importance for the appropriate characterization of the dispersion of pollutants as well as for the noise emission of light and heavy duty vehicles.

The paper is organized as follows. In section 2 we describe the model, the wind tunnel and the experimental technique. In section 3 we present the obtained results in terms of drag and pressure distribution. Furthermore, we focus on the near wake flow field topology and on the modal analysis of the wake. In section 4 we propose a revised model to obtain the optimal number of vehicles in the convoy to maximize the drag reduction. Finally, we draw our conclusions.

2. Experimental setup and measurement techniques

The model is a 3D printed $1:10$ scaled light commercial vehicle, with length (L), width (W) and height (H) equal to 412 mm, 170 mm and 200 mm, respectively. The selected geometry is representative of an existing light commercial vehicle currently manufactured by Fiat FCA. A schematic of the model is shown in Figure 1. The tests were performed in an open-circuit wind tunnel at the laboratory of Aerodynamics "Modesto Panetti" at Politecnico di Torino. The test section of the wind tunnel has a height of 900mm, width of 1200mm and length of 6500mm. When the model is mounted in the wind tunnel, the resulting blockage is less than 3.5%.

The freestream speed (V_∞) is set to $9\ m/s$ corresponding to a Reynolds number based on the model's length $Re_L = \frac{\rho V_\infty L}{\mu} = 230000$. The Reynolds number independence was ensured by investigating a broader range of freestream speeds and checking the variation of the drag coefficient. The results confirmed only minimal variations of the drag coefficient for a 30% reduction of a freestream speed.

The model is positioned within the test section at a distance from the inlet equal to 1900mm, as sketched in Figure 1. The experimental setup is the same as the one reported in Cerutti et al. (2019) Cerutti et al. (2020), Cafiero et al. (2019).

The model is instrumented with 64 pressure taps that populate its lateral and rear surfaces, as schematically depicted in Figure 1 by the red dots. Furthermore, pressure taps are also located in the symmetry plane of the model. The pressure taps are connected to a Scanivalve ZOC 33 pressure transducer interfaced with a PC via TCP/IP protocol. Sixteen microphones in pin-hole configuration, reported in blue in Figure 1, are mounted on half of the base of the model. The signal of these microphones were calibrated using a high quality Bruel & Kjaer probe, as described by Sardu et al. (2015).

The incoming boundary layer profile was characterized in the case of an isolated model. In order to minimize the boundary layer thickness on the wind tunnel floor, a suction slit was located $1L$ upstream of the model. The suction speed was fixed at $V_S/V_\infty = 1$. The incoming boundary layer developing on the wind tunnel floor was measured using a hot wire probe positioned at a distance $x/L = 0.1$ ahead of the model. The boundary layer displacement thickness (δ^*) compared to the ground clearance is $\delta^*/G = 0.07$, which is in good agreement with other investigations on commercial vehicle's aerodynamics (Castelain et al. (2018); Hucho (1993)).We also checked the influence of the suction of the boundary layer on the drag coefficient of the isolated model and found that the drag coefficient without and with suction are different only by less than 2%.

The model is connected through a hollowed beam to a load cell (Dacell UU-K002 load cell, full scale of 2 Kgf and accuracy equal to 0.002%FS). The mounting configuration is shown in Figure 1b. The beam is enclosed within an aerodynamically shaped hull, as a NACA0018 profile.

The voltage signals from the load cell and the pressure fluctuations sensors were sampled by a National Instruments data acquisition board characterized by A/D resolution of $16bit$. The drag measurements were performed taking into account a total sampling time of three minutes to ensure statistical convergence.

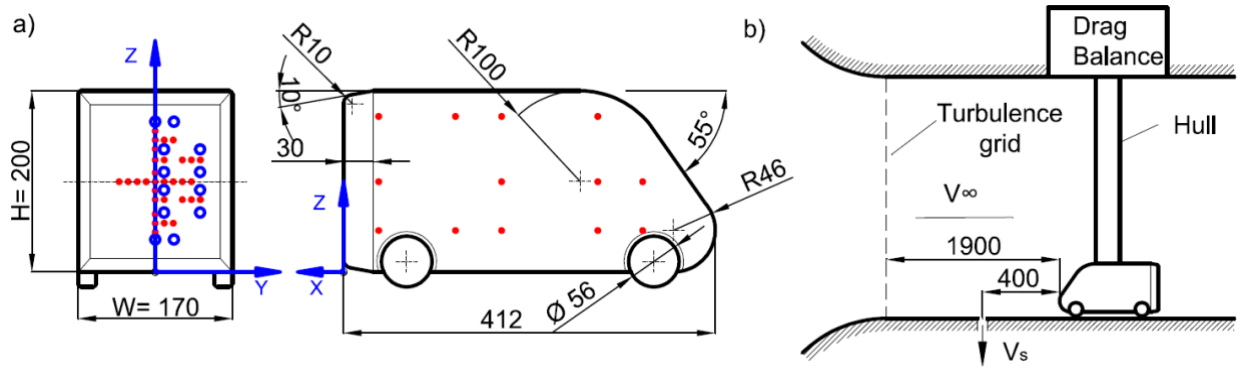

Figure 1: a) Schematic representation of the model with indication of the location of the pressure taps (red) and microphones (blue). b) Sketch of the model's positioning in the test section, with schematic representation of the location of the drag balance and the boundary layer suction slit. Drawing not to scale.

The platoon configurations are reproduced using three equal non-instrumented dummy models. Given the length of the test section as well as the length of the van model, non-dimensional distances ranging from $d/L = 0.125$ to $d/L = 3$ were investigated.

Planar PIV (2D2C) measurements were performed for the two-model platoon and focused on the investigation of the symmetry plane of the model (XZ). The illumination of the tracer particles is obtained using a Dantec Dynamics Dual Power Nd:YAG laser characterized by 200mJ/pulse and 15Hz maximum repetition rate. The laser beam was shaped into a sheet having a thickness of about 1mm, using a spherical and a cylindrical lens. The PIV images were captured using one Andor sCMOS 5.5Mpix camera equipped with a Tokina 100mm Macro lens operated at an aperture $f_{\#}$=16. The resulting digital resolution is about 10pix/mm. In order to ensure a typical displacement between the two frames of about 12 pixels, the time delay between the two laser pulses was fixed to 140μs. For each test, 3000 images were captured to ensure the convergence of the relevant statistics.

The background image as well as the historical minimum is removed from the PIV images to attenuate the effect of laser reflections on the wind tunnel walls and on the model. Images deformation and velocity vector fields interpolation are carried out using spline functions (Astarita (2006), (2008)). A Blackmann weighting window is used during the correlation process to tune the spatial resolution of the PIV process (Astarita (2007)). A multi-step algorithm is implemented to perform the cross-correlation. The initial interrogation window size of 48x48 pixel is reduced down to 24x24 pixel, corresponding to 2.4x2.4mm (i.e. 68 independent vectors across the model's width), with 75% overlap. Considering the typical error in the detection of the correlation peak in the PIV process, we can estimate the velocity vector to be accurate to within 1% of their value.

3. Results

In this section we start by discussing the results in terms of drag reduction obtained in a platoon constituted by 2 vehicles. We also report the pressure distributions, the flow field organization of the near wake and the spectral analysis of the pressure fluctuations. In addition to this, we present the analysis reporting the drag variations for 3 and 4 models in platoon configurations.

Here and in the following the reference frame is defined such that the X axis is aligned with the streamwise direction, the Z axis is aligned with the vertical direction (pointing upwards from the wind tunnel floor) and Y completes the triad.

3.1. Drag variation and pressure distribution

The percentage drag variation $\Delta C_D\% = (1 - C_D^p/C_D)$, with C_D being the drag coefficient of the isolated case and C_D^p the drag coefficient in the platoon configuration, is reported in Figure 2a as a function of the inter-vehicle distance d/L. As detailed in the previous section, we only had one instrumented model. The dummy

model was alternatingly positioned at different locations ahead or behind it, obtaining the red and blue lines of Figure 2a, respectively. Furthermore, to give a direct grasp of the overall drag associated with the platoon configuration, the average between these two values is also plotted and referred to as overall drag variation (ODV, Zabat et al., 1995):

$$ODV\ \left(n, \frac{d}{L}\right) = \frac{\sum_{i=1}^{n} \Delta C_{D\,i}\%\ \ \left(\frac{d}{L}\right)}{n} \qquad (1)$$

where *n* represent the total number of vehicles, and i indicates the i-th model.

Figure 2a evidences that independently from the value of d/L an overall drag reduction is attained, with a largest value of 35% at d/L=0.125 and the minimum value of 18% at d/L=3.

The rear vehicle benefits of the highest values of drag reduction with a maximum of 70% at d/L=0.125 and 42% at d/L=0.5, with a nearly constant value in the range 0.75<d/L<2.5. The large values of drag reduction on the rear vehicle when the inter-vehicle distance is small are mostly related to the low pressure region originating in the lee of the leading vehicle.

Conversely, the progressive reduction in the drag benefit experienced by the rear model at larger values of the inter-vehicle distance is associated with the vortical structures generated by the leading vehicle; as argued by Pagliarella et al. (2007) the quasi-streamwise structures produced in the near wake of the leading vehicle (Cerutti et al. 2020, Pavia et al. 2018a) increase the pressure on the front of the rear vehicle, thus

progressively reducing the drag benefit. This only occurs for values of d/L sufficiently large to allow the production of the quasi-streamwise structures, namely d/L>0.5.

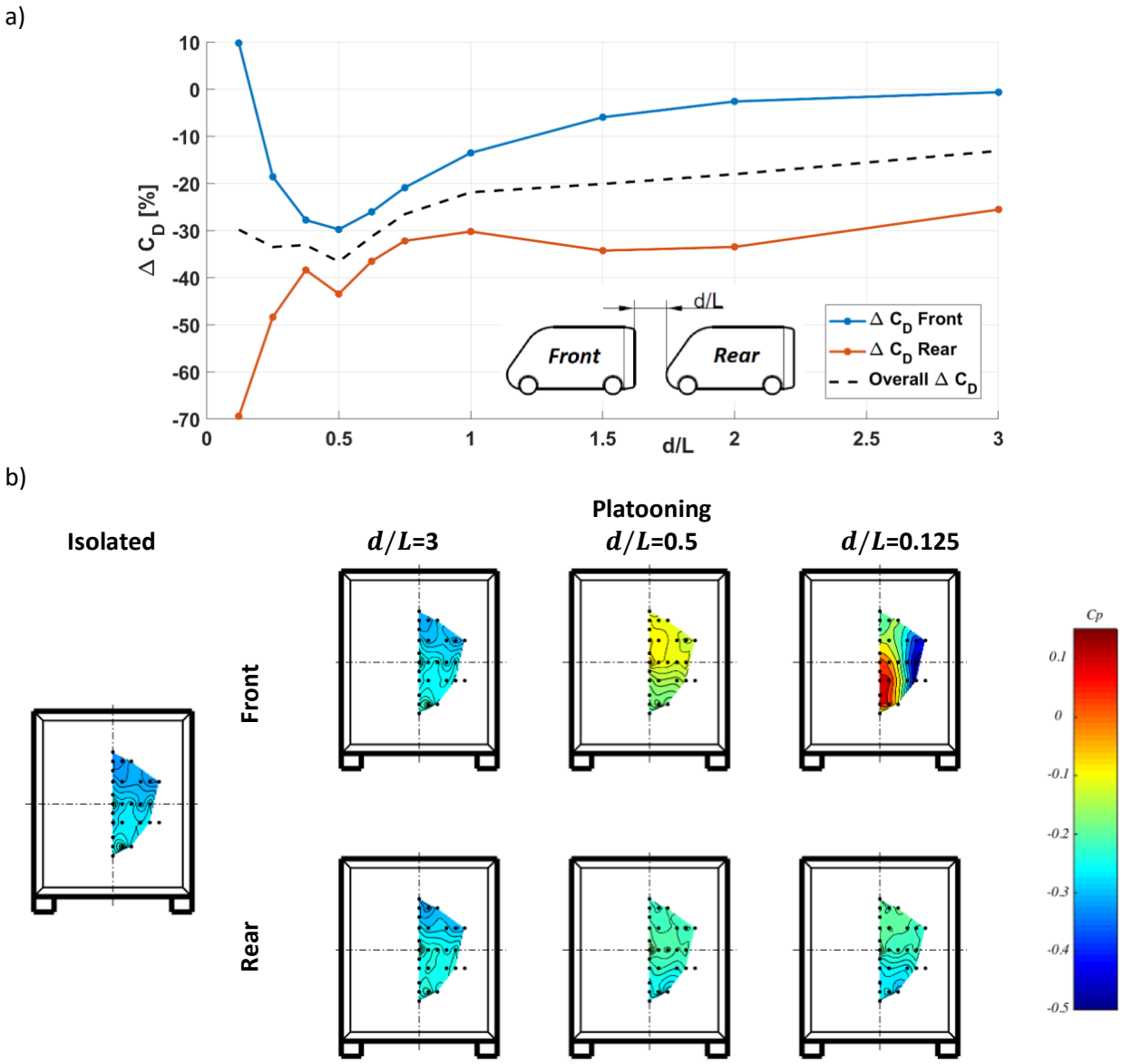

Figure 2: a) Percentage variation of the drag coefficient ΔC_D for the two models platoon configuration as a function of the distance between the models d/L: front model (Blue), rear model (Red), overall drag variation (dashed line). b) Pressure coefficient distribution on the base of the front (top row) and the rear model (bottom row). The isolated case is also reported as a reference. The location of the pressure taps is indicated with black dots. The contour plots are obtained by interpolating the measurements on a structured grid.

The pressure distributions on the model's base (Figure 2b) and along the symmetry plane of the model (Figure 3), expressed in terms of the pressure coefficient $C_p = \frac{(p-p_\infty)}{q_\infty}$, with $q_\infty = \frac{1}{2}\rho V_\infty^2$ being the dynamic pressure, are helpful to understand the results of figure 2a.

As it can be inferred from Figure 2b, for the isolated model the base shows a value of the C_p nearly constant and equal to -0.25 with a downwards directed pressure gradient. Similar observations are valid for the case

of d/L=3, where the mutual interaction of the two models progressively reduces, as also confirmed by the C_D values.

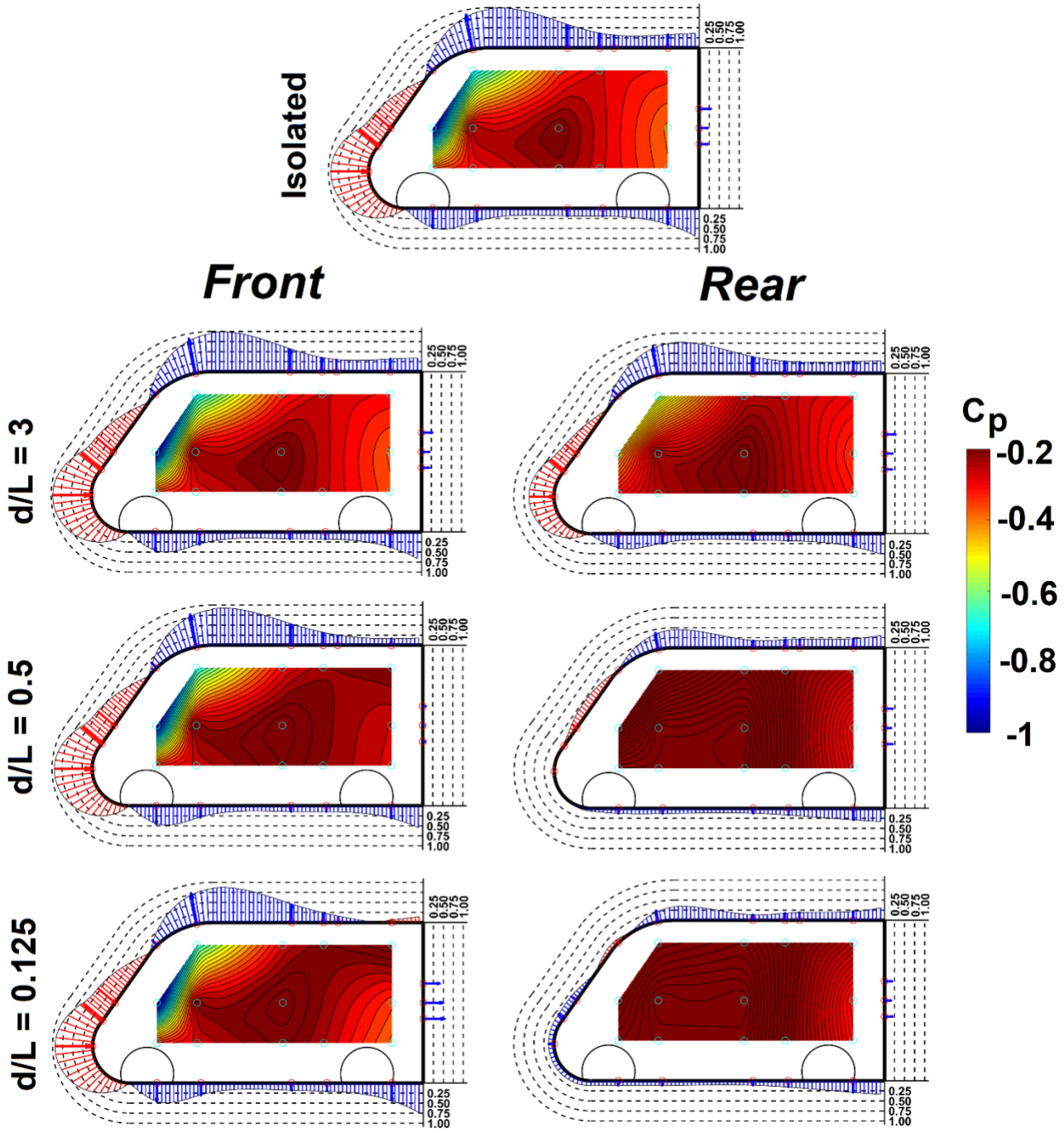

Figure 3: Pressure coefficient distributions for the isolated, front (left) and rear (right) vehicles. Distributions on the lateral surface as a function of the normalised distance d/L. The vector plots represent the value of the pressure coefficient on the roof, front part, rear part and underbody of the vehicle along the symmetry plane. The contour plots are obtained by interpolating the measurements onto a structured grid. Blue and red vectors are related to positive and negative values of the pressure coefficient, respectively.

As the distance between the models reduces, the C_p distribution across the base of the front model appears significantly affected. At d/L=0.5, the pressure gradient across the base switches its orientation, suggesting that the mean direction of the recirculation bubble is reversed because of the effect of the approaching rear vehicle. At the smallest investigated distance, d/L=0.125, the presence of a strong lateral pressure gradient

indicates the disappearance of the recirculation region and that the flow is now preferentially directed laterally, along the Y direction.

As expected, the strong effect that is experienced on the front vehicle is not reflected on the rear one, when d/L varies. However, a closer inspection of Figure 2b reveals that, as d/L reduces, also on the vehicle's base there is evidence of a reversed pressure gradient.

The analysis of the pressure distribution along the model's symmetry plane and its lateral surface (Figure 3) provides further information on the mechanism leading to the drag reduction documented in Figure 2a. The front model does not show any significant variations with respect to the isolated case: the flow withstands a pressure increase in the vicinity of the model's nose, with a pressure decrease occurring on the front slant surface as well as on the underbody of the model.

Conversely, the rear model shows a progressive reduction of the low pressure region occurring on the top surface of the model. As it is also documented by the pressure distribution on the lateral surface of the vehicle, when d/L reduces the flow field configuration is similar to the one that would be obtained by a vehicle of length equal to $2L$, as indicated by the absence of the low pressure region on the front slant that is typical of the nose of isolated vehicles.

Besides with the pressure reduction on the front of the rear model, this also justifies the overall drag reduction experienced in the platooning configuration. It is well known that in the case of an isolated vehicle, conditioning the flow to obtain a wake elongated in the streamwise direction is an effective methodology for drag reduction. This was also recently demonstrated by Minelli et al. (2020) who investigated the suppression of wake's lateral instability using active flow control and found that the resulting wake was extended in the streamwise direction and featured 20% drag reduction. This is also exploited to reduce the pressure drag of bluff bodies with passive methodologies such as boat tailing, or the introduction of short taper on the base of bluff bodies (Perry et al. 2016)

In Figure 4Figure 3 we compare our results in terms of drag coefficient of the front (top) and rear (bottom) vehicle when marching in platoon configuration (C_D) normalised with respect to the drag coefficient of the isolated case (C_{D_0}) to those obtained by (Romberg et al. 1971) using two car models, (Zabat et al. 1994) using two, three and four van models, (Pagliarella et al. 2007) and Watkins & Vino (2008) both using Ahmed bodies. A common feature of all the investigated cases is the loss of effectiveness of the platoon for the front vehicles at values of the inter-vehicle spacing larger than $1L$. The rear vehicle is the one characterized by the largest scatter in the comparison between the available and the literature results; nevertheless, our results are in good agreement with the literature results. The larger scatter in the data regarding the rear vehicle is actually expected, being the data dependent on the characteristics of the separated wake flow generated by the leading vehicle, as well as the effect of the front and rear vehicle geometries (Hammache and Browand 2004). However, the obtained results show sufficient agreement with the literature data, thus providing a reliable validation of our measurements.

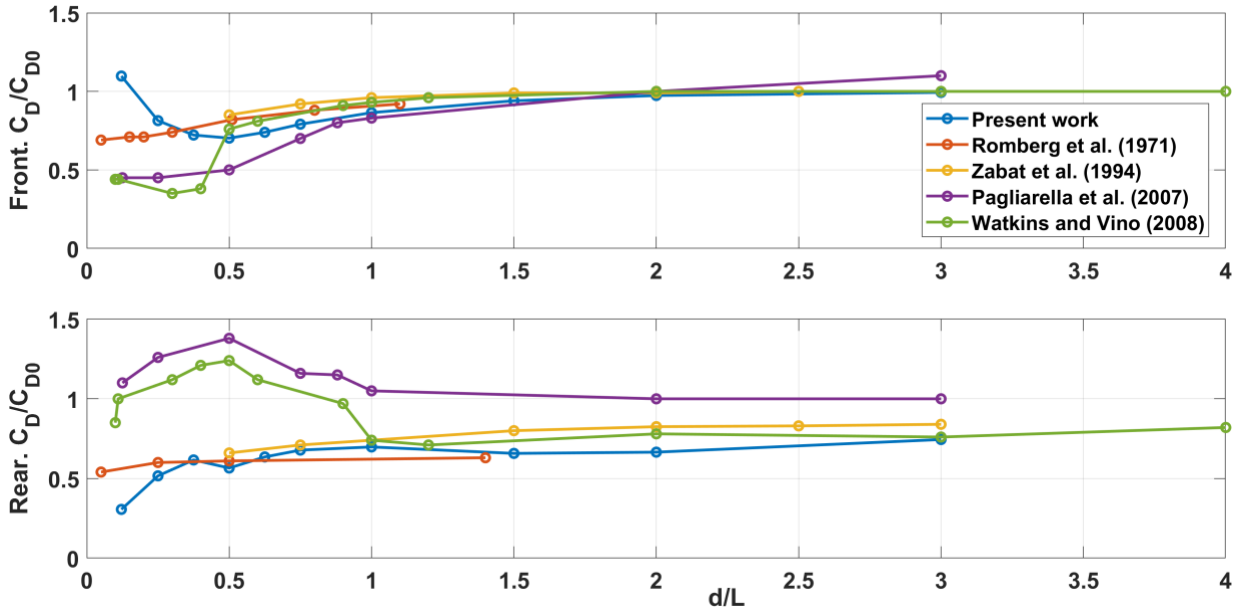

Figure 4: Drag coefficient of the front (top) and rear (bottom) vehicle when marching in platoon configuration (C_D) normalized with respect to the drag coefficient of the isolated case (C_{D_0}) and comparison with available literature using similar models.

3.1.4. PIV analysis: near wake structure of two-van platoon

We now turn our attention to the investigation of the flow field in the wake of the leading and rear vehicle when marching in platoon configuration, at values of d/L=0.125, 0.5, 3 and in the isolated case (as reference). We are particularly interested in evidencing the effect of the platooning on the large scale structures and their organization as a function of d/L.

In Figure 5Figure 6 are presented the contour representations of the time averaged streamwise velocity component U normalised with respect to the freestream velocity V_∞ for the front and the rear vehicles, respectively, obtained in the symmetry plane of the model (Y/W=0). The isolated case is also reported as a reference.

The isolated case features the typical near wake structure of square back bodies (with H/W>1), with an asymmetric recirculation region and two counter rotating structures: a large one located near the top end of the model's base (V2) and a smaller one (V1), whose core is slightly displaced downstream, at $X/W \approx 0.5$. The former structure is generated by the flow undergoing separation from the top surface of the vehicle; the latter is associated with the intense shear region between the high momentum underbody flow and the velocity deficit in the vehicle's wake.
A saddle point (S) can be detected at approximately $Z/W = 0.4$. The streamwise extent of the recirculation region, defined as the region of the near wake where the streamwise velocity is less than or equal to zero ($U/V_\infty \leq 0$), is approximately $1W$.
At d/L=3 the wake structure is similar to the one observed in the isolated case. The same behaviour was observed for the base pressure in Figure 2b. A slight upward shift of the saddle point can be detected, which indicates that the near wake is only partly affected by the adverse pressure gradient induced by the rear vehicle.

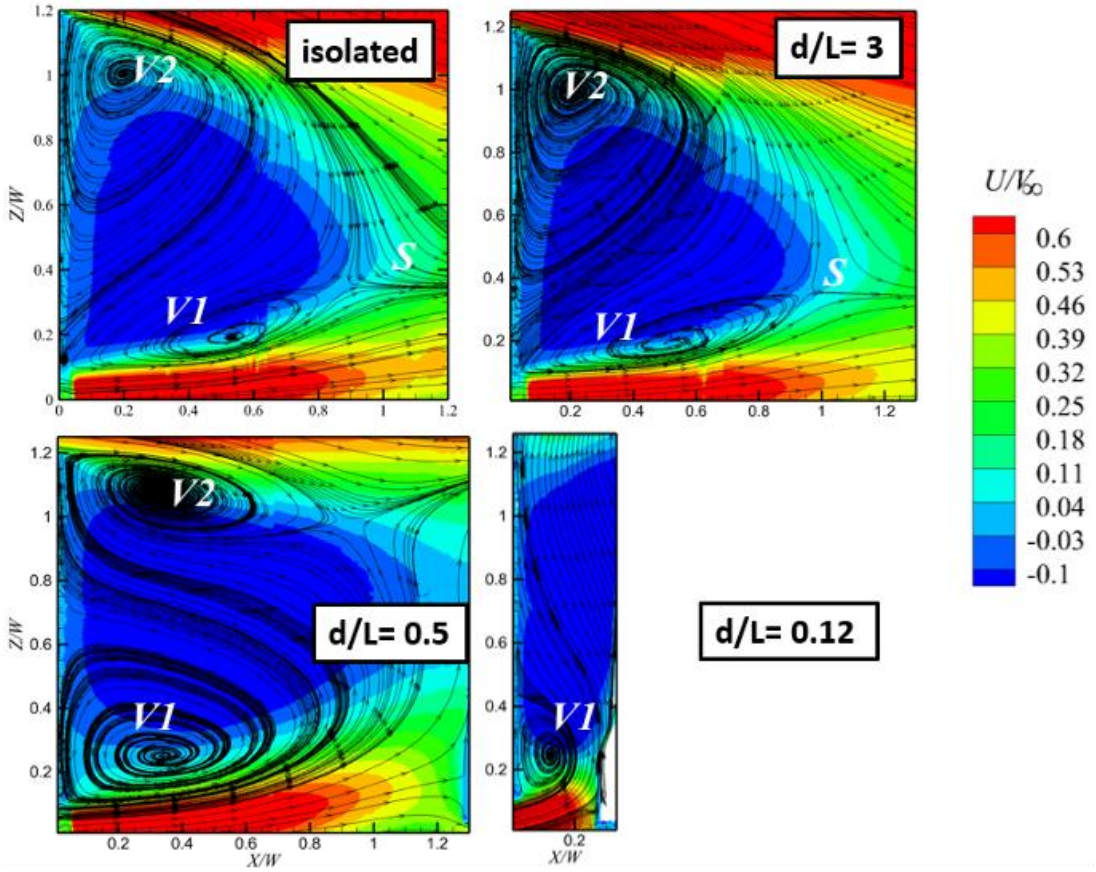

Figure 5: Time averaged wake structure of the front model: contour representation of the dimensionless mean streamwise velocity U/V_∞ with overlaid streamlines. Data are measured in the symmetry plane of the model, Y=0.

As d/L decreases to 0.5, the lower structure (V1) becomes significantly stronger. The approaching rear vehicle forces the flow towards the top surface, which seems to trigger a flow separation on the wind tunnel floor. This results into an upward shift of the saddle point (S) which is now located at $Z/W = 1$. Furthermore, the reversed direction of the pressure gradient evidenced in Figure 2b reflects into the fact that the base is largely dominated by V1, while the top vortex (V2) is progressively pushed upwards.
At the shortest distance, $d/L = 0.125$, a significant distortion of the flow structure can be detected. The adverse pressure gradient induced by the rear vehicle causes the expulsion of both the top vortex (V2) and the saddle point (S). Given the space constraint imposed by the rear vehicle, the lower vortex (V1) is also reduced in size. It must be pointed out that the tendency of the flow to separate from the floor could have an effect on the overall wake balance. However, with the present data it is not possible to determine the extent of this effect.

The wake of the rear vehicle is reported in Figure 6, where we also report the already discussed isolated case for comparison purposes. We indicate as V3 and V4 the bottom and top vortices, respectively. We labelled these structures differently from V1 and V2 in the isolated case to avoid confusion when the inter-vehicle distance reduces. However, it must be stressed that, only in the case of isolated vehicle, V3≡V1 and V4≡V2. At inter-vehicle distance d/L=3, the near wake shows some significant differences with respect to the isolated case: the wake exhibits a nearly symmetric configuration, with the lower vortex (V3) featuring a substantial growth. The saddle point (S) is consequently shifted upwards to $Z/W = 0.5$. This behaviour can be addressed to the less energetic underbody flow in the case of platoon configuration, thus allowing an upstream shift of the bottom vortex towards the model's base.

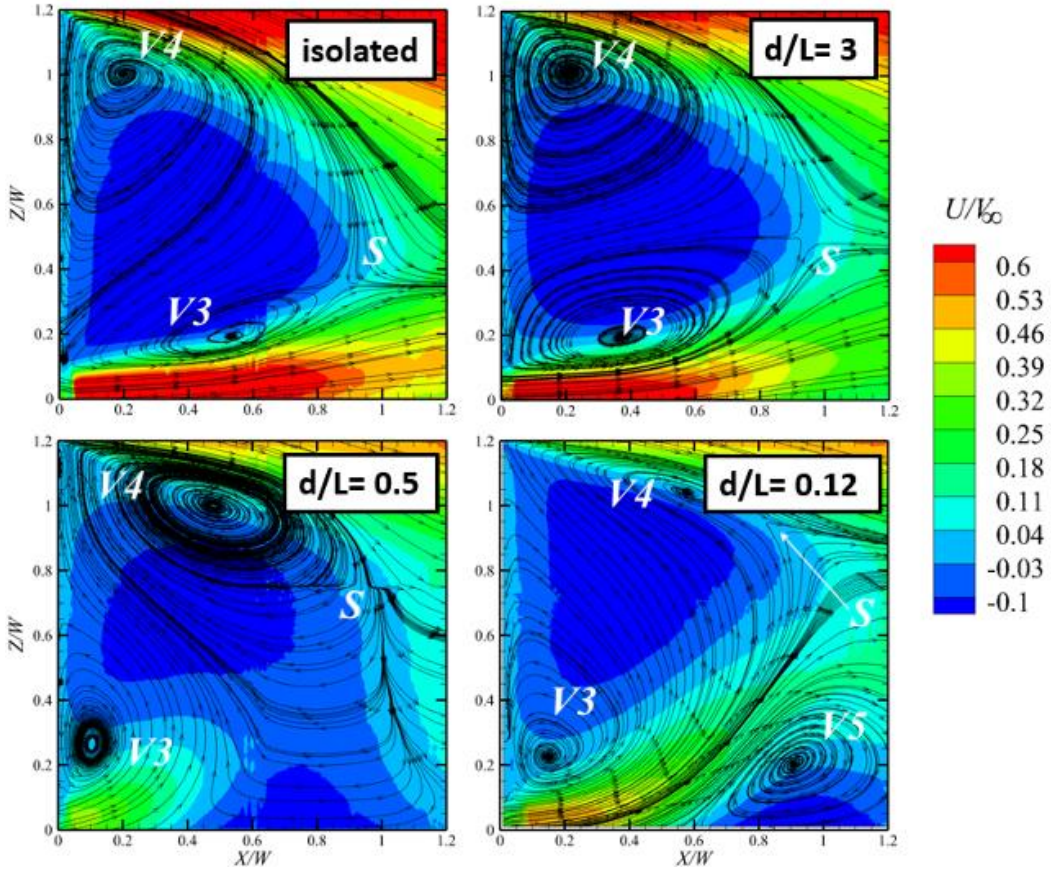

Figure 6: Time averaged wake structure of the rear model: contour representation of the dimensionless mean streamwise velocity U/V_∞ with overlaid streamlines. Data are measured in the symmetry plane of the model, Y=0.

At d/L=0.5, the near wake of the rear vehicle is substantially affected by the different topology of the incoming flow. The interplay between the underbody flow and the one that undergoes the pressure reduction on the top surface of the model generates a large recirculation region with a core centred at $Z/W = 1$ and displaced downstream ($X/W = 0.5$) and results to be elongated towards the wind tunnel floor. The lower structure is attached to the base and reduced in size and enclosed by the larger top structure.

At the smallest inter-vehicle distance investigated, d/L=0.125, the effect of the flow undergoing the pressure reduction on the vehicle's roof significantly affects the rear wake topology. As observed in Figure 6, at d/L=0.125 the flow is forced towards the vehicle's roof, generating a flow separation from the wind tunnel floor on the aft part of the rear vehicle. The low momentum fluid in the wake of the rear vehicle is entrained within the flow coming from the vehicle's roof, effectively causing: (i) an alteration of the top vortex (V4), which reduces its size and gives way to the growth of the lower structure (V3); (ii) a flow separation (V5). This feature, that is found also in the isolated case for similar values of the non-dimensional ground clearance (G/W, Grandemange et al., 2013a) at larger distances from the vehicle (X/W=1.5), occurs much closer to the base in platooning configuration.

The base pressure associated to the latter wake configuration (Figure 2b), along with the separated flow on the front part of the vehicle gives rise to highest value of drag reduction, as large as 70%.

3.1.2. Spectral analysis of the pressure signals

The time series recorded by the microphonic probes mounted on the model's base were analysed in the frequency domain to characterize the features of the wake unsteadiness. Three representative pressure taps were considered, located near the top, right and bottom edge of the base, as schematically represented in Figure 7.

In Figure 8 we report the power spectral density (PSD) in the case of the front and rear vehicle for values of d/L=0.125, 0.5, 3 and isolated wake.

In the isolated case, the PSD shows a peak at a value of the Strouhal number $St = fW/V_\infty \approx$0.12. This value is typical of the vortex shedding phenomenon from a broad range of bluff bodies, as widely documented in the literature (Grandemange et al. (2013), Volpe et al. (2015), and Pavia et al. (2018)).

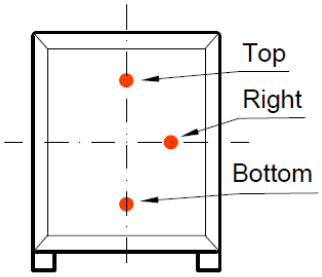

Figure 7: Schematic representation of the location of the reference microphones.

The PSD of the front vehicle shows increasing and broader levels of the spectral energy as the rear vehicle approaches; it is then possible to argue that the near wake in platoon configuration is generally more turbulent than the equivalent isolated case. While this increase affects the whole range of measured non-dimensional frequencies for the right and bottom microphones, featuring a broadband increase of the PSD intensity with respect to the other values of d/L, in the case of the top microphone a large share of the spectral energy is associated with the high frequencies; this suggests that at d/L=0.125 the flow is characterized by smaller scale structures with respect to the other cases. It is also relevant to notice that for the front vehicle the peak associated with the vortex shedding is progressively suppressed when d/L decreases.

The pressure fluctuation signals measured on the base of the rear vehicle show much less dependence on d/L, with values of the PSD very close to the isolated wake. The only exception is related to the bottom microphone at d/L=0.125, where the PSD shows an intensity reduction across the whole range of investigated frequencies. While this may seem surprising, it is possible to argue that the strong differences experienced in the near wake of the rear vehicle are mostly associated with features that are located further downstream, with an effective lower activity in the close proximity of the base.

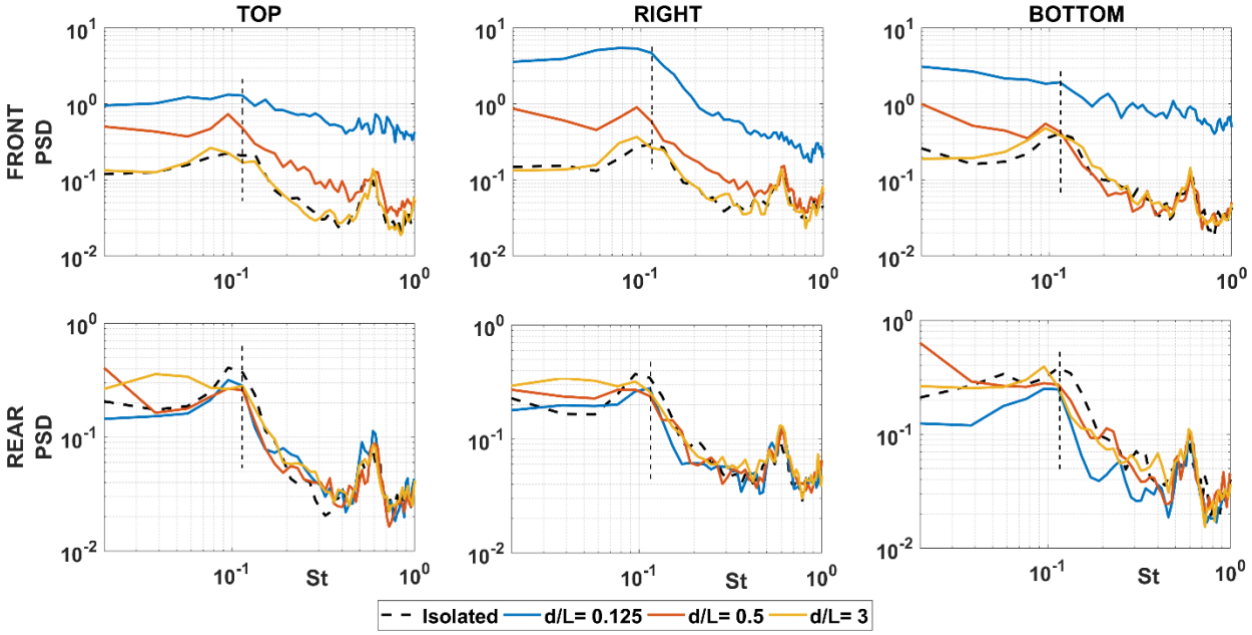

Figure 8: Power spectral density of the pressure taps' fluctuations in three representative locations of the base. Data are shown for the front and rear vehicle at values of $d/L = 3$, $d/L = 0.5$, $d/L = 0.125$. The isolated case is also reported as reference.

It is also worth to mention that, for all the investigated cases, a second peak occurs at $St \approx 0.7$. Identifying the origin of such peak is not straightforward. It is the authors' opinion that this high frequency peak is associated with small scale structures generated in the shear region between the low momentum recirculation bubble and the incoming flow from the vehicle's roof.

3.1.3. Proper orthogonal decomposition analysis of the pressure fluctuations

The simultaneous measurements of the twelve microphones across the model's base were used to perform a Proper Orthogonal Decomposition (POD)-based analysis. The purpose of this analysis is twofold: firstly, it allows us to determine the most energetic modes in the isolated case, serving the purpose of comparison with the literature; secondly, it allows us to determine what is the effect of the distance d/L on the wake's most energetic modes.

The POD technique decomposes a temporal signal into modes and modal coefficients, as explained by Berkooz et al. (1993). This decomposition considers that a given signal $p'(Y,Z,t)$ may be decomposed into the sum of a number of modes k, which are constituted by a temporal coefficient $a_k(t)$ and a spatial eigenfunction $\varphi_k(Y,Z)$ as follows:

$$p'(Y,Z,t) = \sum_k a_k(t)\varphi_k(Y,Z) \quad (3)$$

The eigenfunctions $\varphi_K(x,y)$ need to satisfy the condition

$$\int \langle p'(Y,Z,t) \cdot p'(Y,Z,t)^T \rangle_t \cdot \varphi_j(Y,Z) dydz = \lambda_j \cdot \varphi_j(Y,Z) \quad (4)$$

where j ranges from 1 to the total number of microphones, 12.

Figure 10-Figure 9 show the first four POD modes across the base of the vehicle in the isolated case (first row) and for values of d/L =3, 0.5 and 0.125, for the front and rear vehicle, respectively.

In the isolated case, the first and most energetic mode is a flat mode, often referred to as pumping, characterized by a low frequency streamwise oscillation of the whole wake. Second and third mode, are representative of a vertical symmetry breaking (VSB) mode and horizontal symmetry breaking (HSB) mode, which are associated with the top down and right left shedding of the wake. Similar results were evidenced by Pavia et al. (2018).
Across the base of the front vehicle, while the pumping mode is retained at d/L=3 and d/L=0.5, at the shortest distance it is replaced by an HSB mode. As it was observed from the time averaged flow field results, the wake at d/L=0.125 is significantly affected and, in the symmetry plane Y/W=0, undergoes a preferential bottom-top evolution. This also suggests that the most relevant shedding mechanism surviving the adverse pressure gradient imposed by the rear vehicle is the horizontal one.

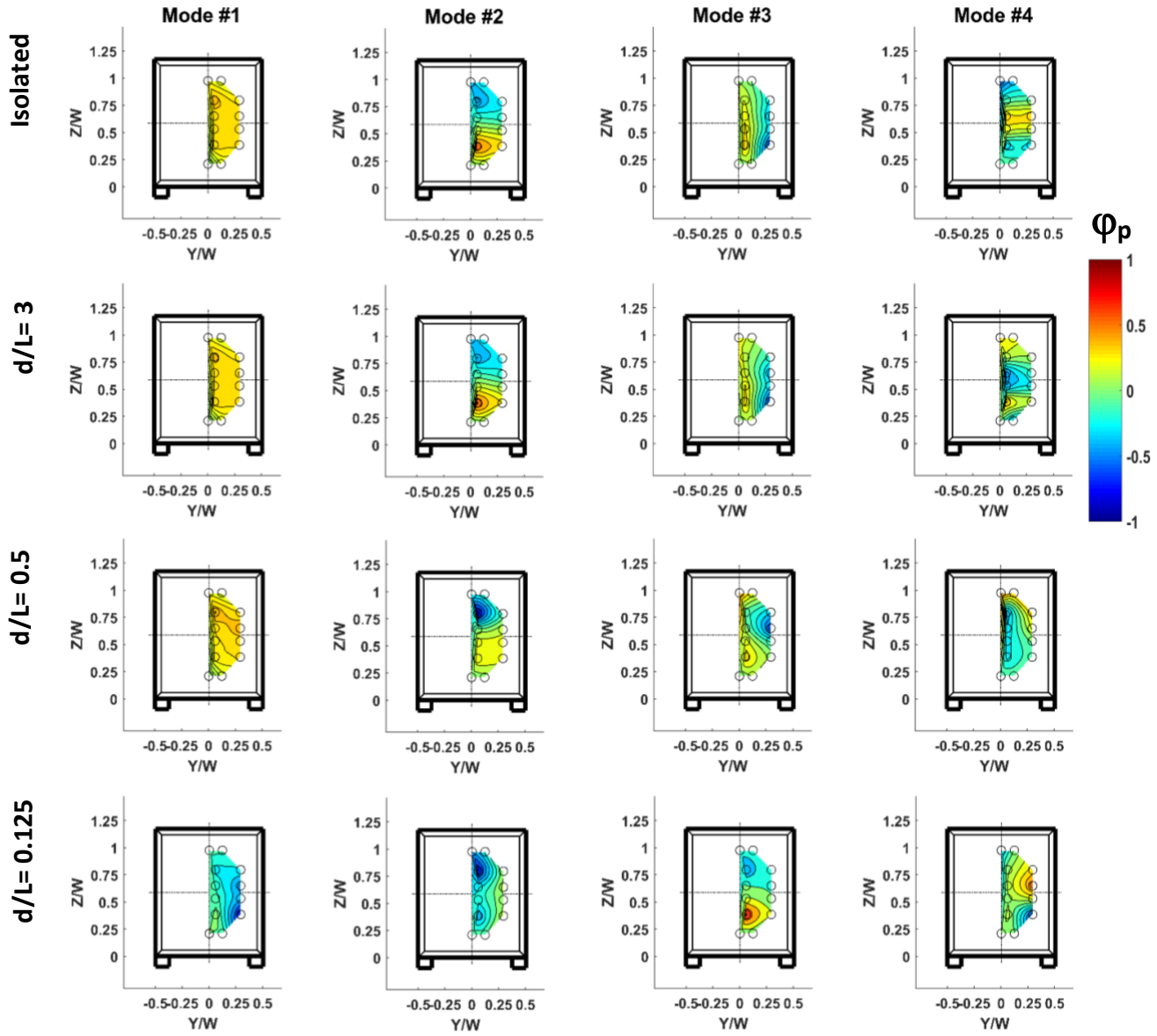

Figure 9: POD analysis applied to the pressure signals for the front model. Contour plots obtained for the cases of isolated vehicle and d/L=3, d/L=0.5 and d/L=0.125.

Furthermore, the expulsion of the structure originating near the top edge of the base (V2) evidenced by the flow field results of Figure 6 along with the disappearance of the flat mode in the POD results of Figure 9 suggest that this structure can be considered as the main responsible for the pumping mechanism. A different behaviour is also observed in the case of d/L=0.5 for the modes 3 and 4, where the HSB and the symmetric modes observed in the isolated and d/L=3 cases are replaced by more complex patterns.

From Figure 10 we can immediately observe that, in the case of the rear vehicle, the modes are not significantly affected by the value of d/L.

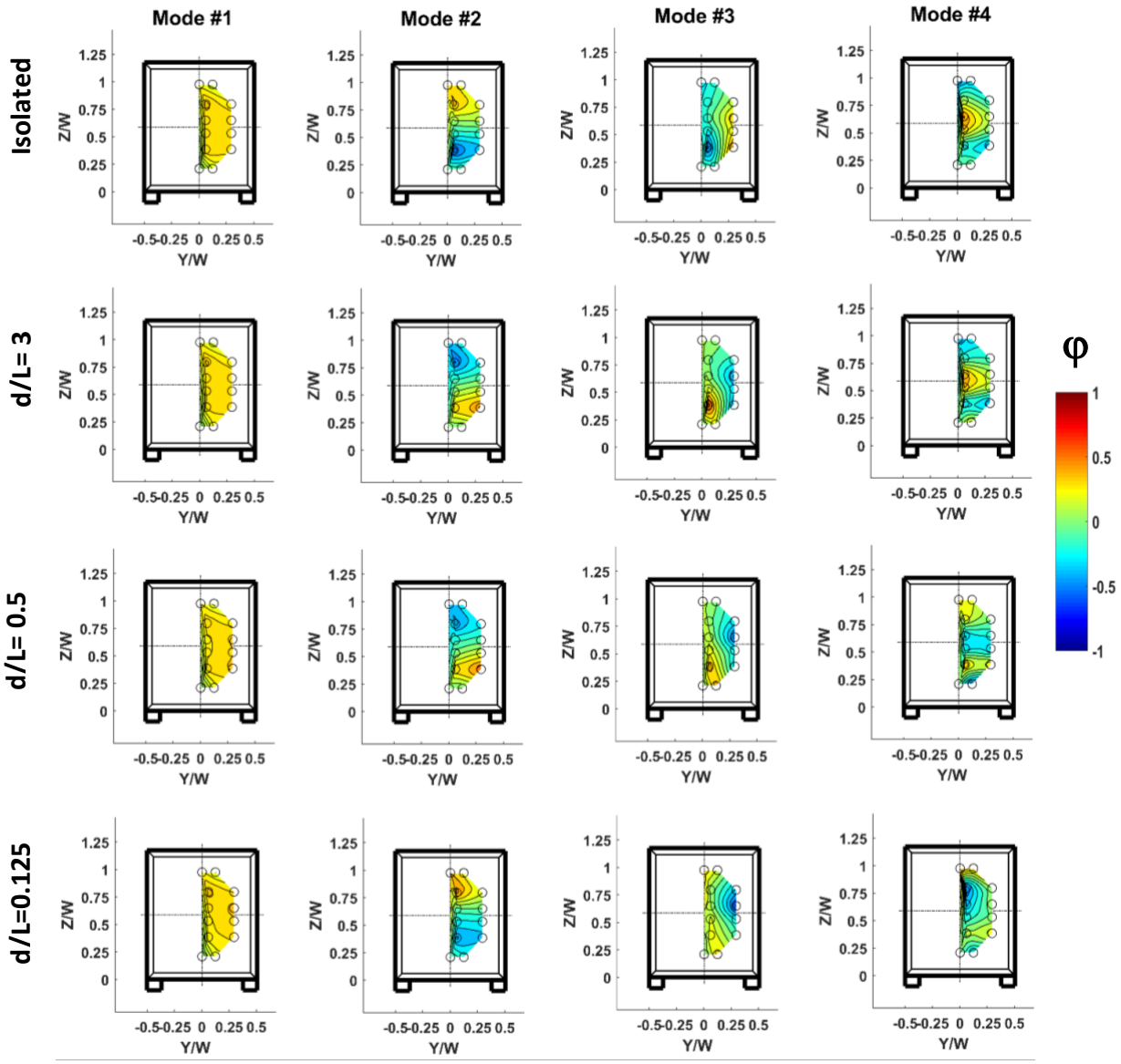

Figure 10: POD analysis applied to the pressure signals measured on the base of the rear model. Contour plots obtained for the cases of isolated vehicle and d/L=3, d/L=0.5 and d/L=0.125.

The comments for the isolated case will then be extended also to the other cases.
The only remarkable difference on the rear vehicle is obtained in the analysis of the fourth mode. While the isolated case, as well as d/L=3 and 0.5 show a symmetric mode (suggesting in-phase shedding), at d/L=0.125 the fourth mode exhibits a more complex behaviour which cannot be referred to neither as symmetric nor asymmetric mode.

Besides the qualitative representation, it is also relevant to underline how the energy is distributed across these four modes, depending on the value of d/L. In Figure 11 the energy distributions of the POD modes are shown for the front and rear vehicles. As it can be observed, the first four modes account for about 95% of the total energy.
For the front model, at d/L=3 (Figure 11a) no significant differences can be detected with respect to the isolated case on the way the energy is distributed across the modes, in good agreement with the flow field and pressure distribution results.
For values of d/L<3, the first mode shows decreasing values of energy: this is expected since the top vortex (V2), that we associate to the pumping mechanism, is progressively reduced as d/L reduces and disappears

when d/L=0.125. This share of modal energy is eventually distributed across the higher order modes, evidencing a more uniform distribution as d/L decreases.
For the rear model, in the light of the results of Figure 10, the only relevant difference in the way the energy is distributed across the most energetic modes is observed at d/L=3. The first mode results much more energetic than the other cases. As observed from the time-averaged PIV results this case is characterized by a symmetric configuration with the sizes of the top and bottom structures being comparable, which might justify this energy enhancement. However, the current results do not allow to draw a clear conclusion on this point which will remain open for future investigations.

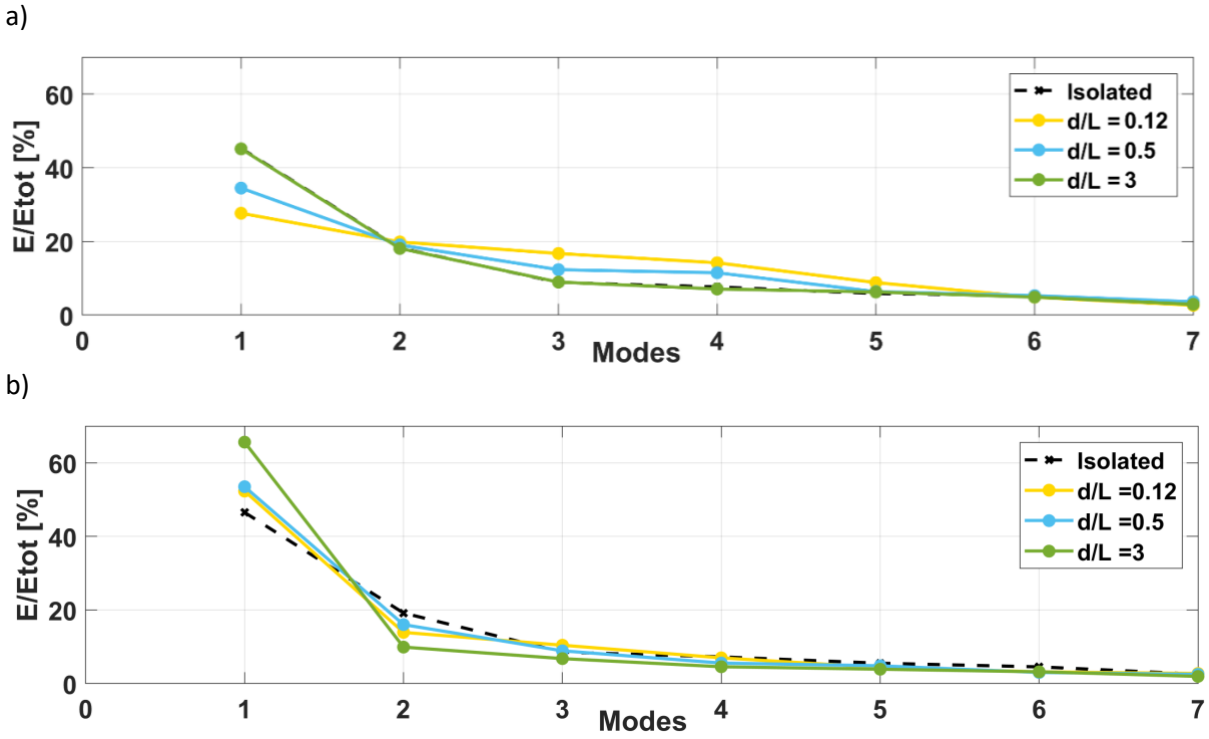

Figure 11: Energy of the POD modes normalised with respect to the total modal energy of the flow: a) front model and b) rear model. The dashed lines refer to the isolated vehicle.

3.2. Three and four-van platooning

Figure 12 shows the percentage drag variation of the platoon configuration when three (a) and four (b) vehicles are considered, respectively. Given the limitations imposed by the size of the test section, the maximum allowed distance between models is $d/L = 1.5$. Despite this limitation, the results allow to make significant observations about the benefits that can be obtained in the platoon configuration.
As it can be seen from Figure 2: a) Percentage variation of the drag coefficient ΔC_D for the two models platoon configuration as a function of the distance between the models d/L: front model (Blue), rear model (Red), overall drag variation (dashed line). b) Pressure coefficient distribution on the base of the front (top row) and the rear model (bottom row). The isolated case is also reported as a reference. The location of the pressure taps is indicated with black dots. The contour plots are obtained by interpolating the measurements on a structured grid.

a and b, the presence of more vehicles in the platoon is associated with a drag increase for the trailing vehicle, which makes this last location the least favourable in the platoon. In fact, those vehicles which are located in the middle are those which exhibit the highest values of drag reduction (model 2 in Figure 12a and model 2 and 3 in Figure 12b). Conversely, the front model does not show any significant dependency on the number of elements in the platoon.

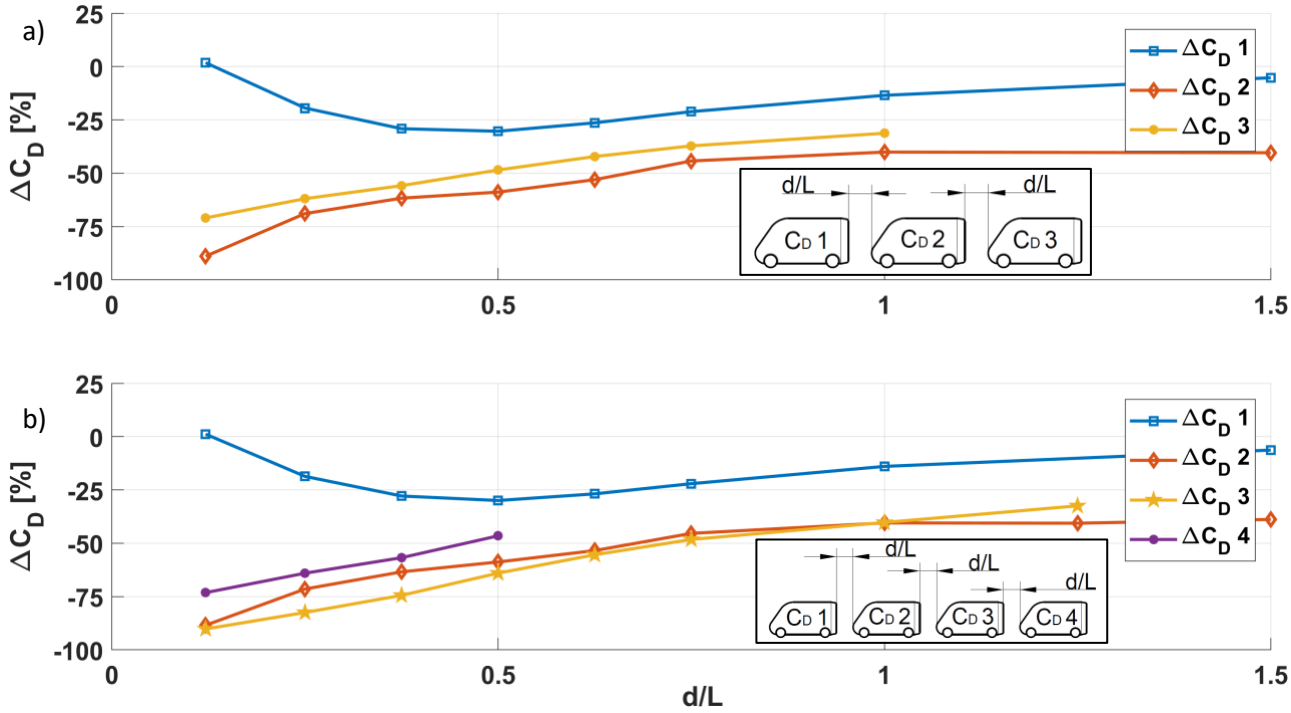

Figure 12: Percentage variation of the drag coefficient ΔC_D for the (a) three-models platoon and (b) four-models platoon configurations as a function of the distance between the models d/L.

In the case of three vehicles (Figure 12a) the middle one benefits of a further share of drag reduction of about 5% with respect to the rear vehicle and 15% with respect to the front one. This result is found quite independent on the value of the inter-vehicle distance.

In the case of four models, the two intermediate vehicles benefit from the highest drag reductions, evidencing an extremely similar behaviour and reaching at d/L=0.125 the same drag reduction (85%) of the middle vehicle for the case with three vehicles.

Figure 12 shows that, as the number of vehicles in the platoon increases, the drag variation for the intermediate vehicles is independent from the total number of vehicles in the platoon, thus paving the way to the modelling of the drag reduction obtained by a generic n-vehicles platoon. This simplistic model is indeed based on the idea that the intermediate vehicles will be characterized by the same values of drag reduction independently from the value of n. This aspect will be further expanded in the next section.

A last remark is related to the drag reduction associated with small values of d/L. In the light of the advancements in autonomous driving, the close proximity might represent a solid possibility leading to significant values of drag reductions if appropriately exploited. However, in the current scenario, this path can be hardly considered as the high benefit evidenced in terms of drag reductions could be overthrown by safety and hazard concerns.

4. A simple modelling for a convoy with n-vehicles

The investigation in a wind tunnel on the platooning configuration is limited by the maximum number of vehicles that the length of the test section allows. In order to compensate this, Zabat et al. (1995) developed an overall drag variation law for a generic platoon with n-vehicles.

Considering the data from the front, middle and rear vehicles of the 3 and 4 vehicles platoon configurations reported in Figure 12, and the result of Figure 4 showing that for d/L=5 there is no significant effect in terms of drag reduction ($\%\Delta C_D$=0) for the two vehicles convoy, it is possible to perform a best fit using a spline function of these data as shown in Figure 13a. In particular, all the front, rear and intermediate vehicles' data, independently on the number of vehicles in the convoy, where considered and used for the fit.

Under these assumptions, the overall drag variation can be written as:

$$ODV(d/L,n) = \frac{\Delta D_{Front}\left(\frac{d}{L}\right)+\Delta V_{Rear}\left(\frac{d}{L}\right)+(n-2)\Delta V_{Middle}\left(\frac{d}{L}\right)}{n} \quad (5)$$

where $ODV(d/L,n)$ is the overall drag variation for a constant distance d/L between models and for a number of vehicles equal to n. $\Delta V_{Front}\left(\frac{d}{L}\right)$, $\Delta V_{Tail}\left(\frac{d}{L}\right)$ and $\Delta V_{Middle}\left(\frac{d}{L}\right)$ are the drag variations at a value of d/L of the front, rear and intermediate models, respectively.

a)

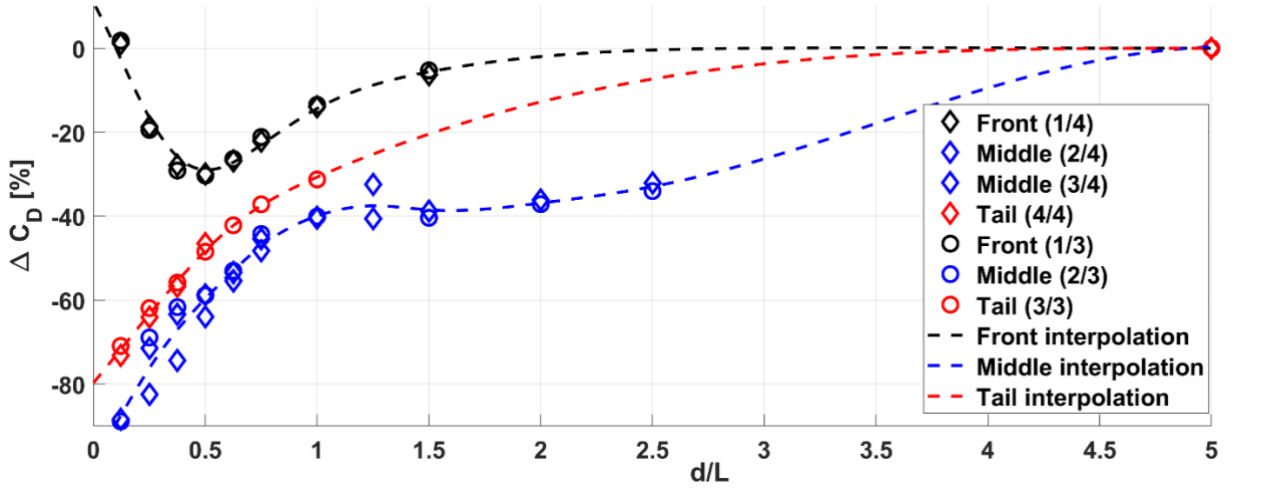

b)

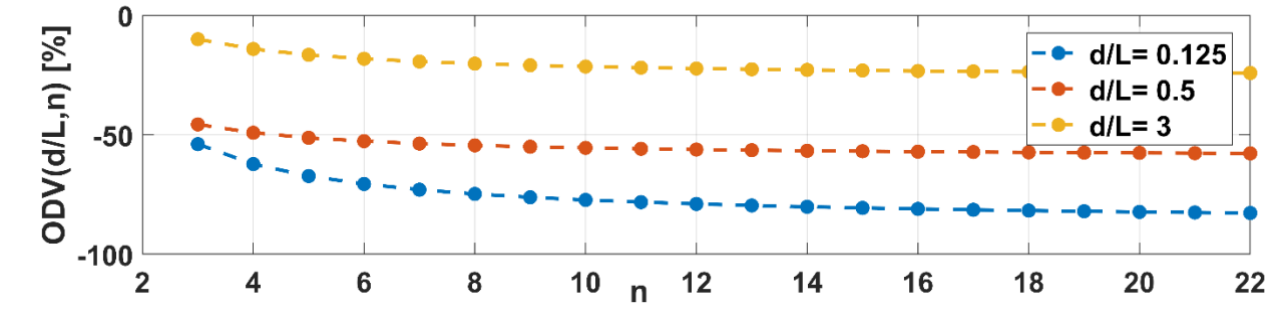

c)

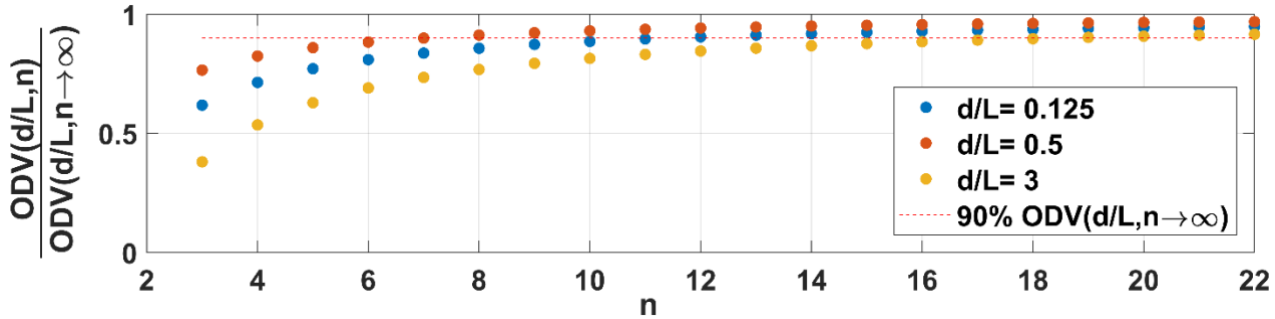

Figure 13: a) Percentage drag variation for the front, tail and middle vehicles as a function of d/L for the two, three and four vehicles' platoon; the dashed lines are representative of the spline interpolation of the data, assuming that at d/L=5 the drag variation is equal to zero. b) Overall drag variation plotted for an increasing number of vehicles in the platoon n and fixed values of d/L=0.125, d/L=0.5 and d/L=3. c) Overall drag variation for an increasing number of vehicles in the platoon n, rescaled with respect to the value obtained for $n \to \infty$. The dashed red line is representative of a user defined target of drag reduction set to 90% of the maximum possible drag reduction.

Figure 13b shows the overall drag variation for a growing number of models n at fixed values of d/L (0.125, 0.5 and 3). For a number of models n >8, for the analysed values of d/L it is not possible to obtain further improvements of the drag reduction.

As it can be observed, for a given distance d/L the drag reduction increases with the number of vehicles in the platoon reaching an asymptotic value which depends on the value of d/L. The asymptotic value can be calculated from equation 5, for $n \to \infty$ obtaining $ODV\left(\frac{d}{L}\right)_{n\to\infty} = DV_{Middle}\left(\frac{d}{L}\right)$, which is effectively representative of the highest value of drag reduction that could be obtained for that particular configuration. Figure 13c shows the overall drag variations normalized with respect to the asymptotic value pertaining to each value of d/L as a function of the number of vehicles n. This is helpful to determine what is the minimum number of vehicles in the platoon necessary to obtain a given value of the maximum drag reduction, for a fixed value of the distance d/L. For the safety considerations that were previously raised, a 25% drag reduction (90% of the maximum achievable) can be obtained with a convoy of 18 vehicles with inter-vehicle distance equal to d/L=3.

5. Conclusions

An experimental study aimed at determining the flow field characteristics of light commercial road vehicles marching in platoon configuration has been carried out. Drag measurements, as well as pressure distribution and flow field organization in the near wake are considered.

The drag measurements allow us to confirm that the effectiveness of the platooning configuration reduces for inter-vehicle distances d/L>3. This also reflects in the flow field organization observed at d/L=3, as well as in the distribution of the modal energy obtained from the microphonic probes. The range of inter-vehicle distances between 0.5 and 1 can be particularly appealing for drag reduction purposes, especially in the light of future advancements in autonomous driving. We show that the presence of a leading edge slant angle, does not affect significantly the drag reduction obtained on the leading vehicle of the platoon. However, the comparison with literature results suggests that the drag reduction attainable by the rear vehicle can be dependent on the leading edge slant angle.

We detail the flow field structures that can be observed in the two vehicle platoon configuration and see that the effect of the reduction of the inter-vehicle distance on the near wake of the front vehicle is mostly associated with the expulsion of the otherwise dominant vortex (labelled as V2). The joint analysis of the PIV and POD data from the microphonic probes also suggests that the V2 structure is the one responsible for the pumping mechanisms, given that at values of d/L=0.125 there is the suppression of the flat mode.

The nature of the substantial drag reduction of the rear vehicle in the platoon configuration is confirmed to be the reduction of the static pressure on the front of the vehicle. At values of d/L=0.125 the flow is substantially affected by the adverse pressure gradient induced by the rear vehicle and undergoes a bottom-top evolution.

The wake of the front model in platoon configuration is found to be generally more turbulent, with a progressive suppression of the vortex shedding experienced at Sr=0.12 in the isolated case.

In the case of three and four-van platoon, we observe that regardless of the number of vehicles in the platoon, the intermediate vehicles show similar values of drag reduction. We use this information to extrapolate the overall drag variation for a growing number of vehicles and quickly determine the minimum number of vehicles necessary to obtain a target value of the drag reduction for a fixed inter-vehicle distance.

The importance of the flow field characterization of vehicles marching in platoon is also confirmed by the strong interest of the research councils which encourage and support research in the field, with the development of dedicated test rigs (TRAIN at the University of Birmingham, for example). Furthermore, the European Union has identified with the smart mobility one of the key drivers of the forthcoming programme Horizon Europe.

In this work, besides providing significant support for previous numerical investigations and exploring a broader range of inter-vehicle distances, we also evidence the importance of future developments in control and autonomous driving. Exploiting the capabilities of the platooning configuration in close proximity might pave the way towards a much more sustainable road transport and to associated reductions in the vehicles' emissions.

References:

Al Alam, Assad, Ather Gattami, Karl H. Johansson, and Claire J. Tomlin. 2011. 44 IFAC Proceedings Volumes (IFAC-PapersOnline) *Establishing Safety for Heavy Duty Vehicle Platooning: A Game Theoretical Approach*. IFAC.

Alam, Assad, Jonas Martensson, and Karl H. Johansson. 2013. "Look-Ahead Cruise Control for Heavy Duty Vehicle Platooning." *IEEE Conference on Intelligent Transportation Systems, Proceedings, ITSC* (Itsc): 928–35.

Astarita, T. 2006. "Analysis of Interpolation Schemes for Image Deformation Methods in PIV: Effect of Noise on the Accuracy and Spatial Resolution." *Experiments in Fluids* 40(6): 977–87.

Astarita, T. 2007. "Analysis of Weighting Windows for Image Deformation Methods in PIV." *Experiments in Fluids* 43(6): 859–72.

Astarita, T. 2008. "Analysis of Velocity Interpolation Schemes for Image Deformation Methods in PIV." *Experiments in Fluids* 45(2): 257–66.

Bergenhem, Carl, Erik Hedin, and Daniel Skarin. 2012. "Vehicle-to-Vehicle Communication for a Platooning System." *Procedia - Social and Behavioral Sciences* 48: 1222–33.

Berkooz, Gal, Philip Holmes, and John L. Lumley. 1993. "The Proper Orthogonal Decomposition in the Analysis of Turbulent Flows." *Annual Review of Fluid Mechanics* 25(1): 539–75. http://www.annualreviews.org/doi/10.1146/annurev.fl.25.010193.002543.

Bonilla, David. 2020. "Road Freight Transport and Energy Use: The USA, China, the EU, Japan and Germany." In , 5–32.

Cafiero, Gioacchino, Juan José Cerutti, and Gaetano Iuso. 2019. "Near Wake Structure of a Square Back Road Vehicle." In *13th International Symposium on Particle Image Velocimetry – ISPIV 2019*,.

Castelain, Thomas et al. 2018. "Identification of Flow Classes in the Wake of a Simplified Truck Model Depending on the Underbody Velocity." *Journal of Wind Engineering and Industrial Aerodynamics* 175: 352–63.

Cerutti, Juan José, Gioacchino Cafiero, and Gaetano Iuso. 2019. "Aerodynamics of Two Square Back Vehicles in Platooning Configuration." In *15th International Conference on Fluid Control, Measurements and Visualization*, Naples (Italy).

Cerutti, Juan José, Costantino Sardu, Gioacchino Cafiero, and Gaetano Iuso. 2020. "Active Flow Control on a Square-Back Road Vehicle." *Fluids* 5(2).

Davila, Arturo, Enric Aramburu, and Alex Freixas. 2013. "Making the Best out of Aerodynamics: Platoons." *SAE Technical Papers* 2: 4–9.

Gehring, Ottmar, and Hans Fritz. 1997. "Practical Results of a Longitudinal Control Concept for Truck Platooning with Vehicle to Vehicle Communication." *IEEE Conference on Intelligent Transportation Systems, Proceedings, ITSC*: 117–22.

Grandemange, M., M. Gohlke, and O. Cadot. 2013a. "Bi-Stability in the Turbulent Wake Past Parallelepiped

Bodies with Various Aspect Ratios and Wall Effects." *Physics of Fluids* 25(9).

Grandemange, M., M. Gohlke, and O. Cadot. 2013b. "Turbulent Wake Past a Three-Dimensional Blunt Body. Part 1. Global Modes and Bi-Stability." *Journal of Fluid Mechanics* 722: 51–84.

Hamiga, Władysław, and Wojciech Ciesielka. 2018. "Numerical Modeling of Airflow over Column of Vehicles Using Ansys® Package." *E3S Web of Conferences* 46: 00025.

Hammache, M, and F Browand. 2004. "On the Aerodynamics of Tractor-Trailers." In *Aerodynamics of Heavy Vehicles:Trucks, Buses and Trains*, , 185–205.

He, Mingzhe et al. 2019. "Detached Eddy Simulation of a Closely Running Lorry Platoon." *Journal of Wind Engineering and Industrial Aerodynamics* 193.

Michaelian, Mark, and Fred Browand. 2000. "Field Experiments Demonstrate Fuel Savings for Close-Following." *University of California at Berkeley*: 25.

Minelli, G., T. Dong, B. R. Noack, and S. Krajnović. 2020. "Upstream Actuation for Bluff-Body Wake Control Driven by a Genetically Inspired Optimization." *Journal of Fluid Mechanics*.

Morel, Thomas. 1984. "Aerodynamics of Road Vehicles." *Fuel Econ in Road Veh Powered by Spark Ignition Engines*: 335–92.

Pagliarella, Riccardo M., Simon Watkins, and Angelo Tempia. 2007. "Aerodynamic Performance of Vehicles in Platoons: The Influence of Backlight Angles." *SAE Technical Papers* 1(724).

Pavia, Giancarlo, Martin Passmore, and Costantino Sardu. 2018a. "Evolution of the Bi-Stable Wake of a Square-Back Automotive Shape." *Experiments in Fluids* 59(1).

Pavia, Giancarlo, Martin Passmore, and Costantino Sardu. 2018b. "Evolution of the Bi-Stable Wake of a Square-Back Automotive Shape." *Experiments in Fluids* 59(1): 20. http://link.springer.com/10.1007/s00348-017-2473-0.

Perry, Anna Kristina, Giancarlo Pavia, and Martin Passmore. 2016. "Influence of Short Rear End Tapers on the Wake of a Simplified Square-Back Vehicle: Wake Topology and Rear Drag." *Experiments in Fluids* 57(11).

Romberg, G. F., F. Chianese, and R. G. Lajoie. 1971. "Aerodynamics of Race Cars in Drafting and Passing Situations." In *SAE Technical Papers*,.

Salari, Kambiz, and Jason Ortega. 2018. "Experimental Investigation of the Aerodynamic Benefits of Truck Platooning." *SAE Technical Papers* 2018-April: 1–11.

Sardu, C., D. Lasagna, and G. Iuso. 2016. "Noise Filtering for Wall-Pressure Fluctuations in Measurements around a Cylinder with Laminar and Turbulent Flow Separation." *Journal of Fluids Engineering, Transactions of the ASME* 138(6).

Tsuei, L., and Ö Savas. 2000. "A Wind Tunnel Investigation of the Transient Aerodynamic Effects on a Four-Car Platoon during Passing Maneuvers." *SAE Technical Papers* 1(724).

Uystepruyst, David, and Siniša Krajnović. 2013. "LES of the Flow around Several Cuboids in a Row." *International Journal of Heat and Fluid Flow* 44: 414–24.

Vegendla, Prasad et al. 2015. "Investigation of Aerodynamic Influence on Truck Platooning." *SAE Technical Papers* 2015-Septe.

Volpe, Raffaele, Philippe Devinant, and Azeddine Kourta. 2015. "Experimental Characterization of the Unsteady Natural Wake of the Full-Scale Square Back Ahmed Body: Flow Bi-Stability and Spectral Analysis." *Experiments in Fluids* 56(5): 1–22.

Watkins, Simon, and Gioacchino Vino. 2008. “The Effect of Vehicle Spacing on the Aerodynamics of a Representative Car Shape.” *Journal of Wind Engineering and Industrial Aerodynamics* 96(6–7): 1232–39.

Yu, Kaijiang, Qing Liang, Junqi Yang, and Yanan Guo. 2016. “Model Predictive Control for Hybrid Electric Vehicle Platooning Using Route Information.” *Proceedings of the Institution of Mechanical Engineers, Part D: Journal of Automobile Engineering* 230(9): 1273–85.

Zabat, Michael, Stefano Frascaroli, and F. K. Browand. 1994. “Drag Measurements on 2, 3 and 4 Car Platoons.” In *SAE Technical Papers*,.

Zabat, Michael, Nick Stabile, Stefano Farascaroli, and Frederick Browand. 1995. “The Aerodynamic Performance Of Platoons: A Final Report.” *California Partners for Advanced Transit and Highways (PATH)*. http://escholarship.org/uc/item/8ph187fw#page-1.